



HAL
open science

Divide-to-Conquer: A Kinetic Model for Singlet Oxygen Photosensitization

Shuming Bai, Mario Barbatti

► **To cite this version:**

Shuming Bai, Mario Barbatti. Divide-to-Conquer: A Kinetic Model for Singlet Oxygen Photosensitization. *Journal of Chemical Theory and Computation*, 2017, 13 (11), pp.5528-5538. 10.1021/acs.jctc.7b00619 . hal-02288768

HAL Id: hal-02288768

<https://amu.hal.science/hal-02288768>

Submitted on 16 Sep 2019

HAL is a multi-disciplinary open access archive for the deposit and dissemination of scientific research documents, whether they are published or not. The documents may come from teaching and research institutions in France or abroad, or from public or private research centers.

L'archive ouverte pluridisciplinaire **HAL**, est destinée au dépôt et à la diffusion de documents scientifiques de niveau recherche, publiés ou non, émanant des établissements d'enseignement et de recherche français ou étrangers, des laboratoires publics ou privés.

Divide to Conquer: A Kinetic Model for Singlet Oxygen Photosensitization

Shuming Bai and Mario Barbatti**

Aix Marseille Univ, CNRS, ICR, Marseille, France.

Abstract

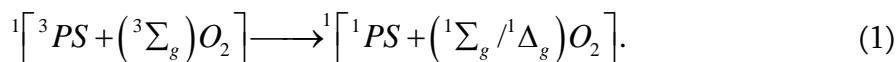
Photosensitized singlet oxygen generation occurring in a PS-O₂ complex, where PS is a photosensitizer chromophore, is a weakly-coupled intermolecular energy-transfer process, a still challenging problem for theoretical chemistry. To investigate the reaction rate directly from quantum chemical calculations, we built a semiclassical kinetic model that minimizes the computational effort for the calculation of diabatic couplings, activation energies, and reorganization energies; which are the components of the rate. The model splits the system into sets of orthogonal coordinates, which are then explored to compute the reaction rate. This model offers an effective way to evaluate the reaction probability of singlet oxygen generation along different directions and intramolecular distances of the PS-O₂ complex. The model can also be applied to

other similar intermolecular energy-transfer problems, to connect the reaction kinetics and quantum chemical calculations.

1 Introduction

For decades, photosensitizers (PS) for singlet oxygen generation have been developed for applications in chemical synthesis and phototherapy.¹ Computational theoretical chemistry has been playing an important role on this topic, by, first, contributing to quantitatively rationalize the empirical relationship between the singlet oxygen generation rate and the properties of photosensitizers² and, secondly, predicting reaction mechanisms.³ Theoretical approaches have been fundamental, for instance, to explain the initial populations of the PS triplet state^{2c, 4} or the effect of triplet state decay on the singlet oxygen generation.⁵ Nevertheless, direct quantum chemical calculation of the photosensitization kinetics is still quite missing (with the noticeable exception of ref. ^{3f}), likely, due to the complexity of the intermolecular energy-transfer problem itself; enhanced by the open-shell character of the system.^{1a, 2a, 6}

During the photosensitization process, the final step, which is responsible for the generation of the singlet oxygen species, takes place through the internal conversion reaction:



There are, indeed, other reactions producing single oxygen through intersystem crossing, but this spin-allowed reaction will dominate the whole rate and becomes the most important one to be investigated.^{2a}

Reaction (1) implies that the photosensitization is an intermolecular energy-transfer problem. The coupling and dynamics of such a process for many different systems have often been investigated employing different levels.⁷ In fact, reaction (1) can be seen as the inverse of the key reaction in singlet fission problems; and we can profit from that. Direct calculation of singlet fission, including different ways to obtain rates and the diabatic coupling between the two states of the complex, has been developed by various groups.⁸ It is reasonable to follow a similar treatment for singlet oxygen photosensitization. Nevertheless, there are two major differences we must face: first, the already mentioned open-shell character of the PS-O₂ complex and, secondly, the different condensed phases of the system. While singlet fission usually takes place in the solid phase, with well-determined structures; singlet oxygen generation happens in solution, involving a broad distribution of intramolecular distances and conformations of floppy complexes.

This large geometric variability, as well as the strong dependency of the coupling strength on these geometries, poses a major challenge for the treatment of this type of problem. As we explain below, we address these issues by splitting the coordinates relative to the intra- and intermolecular motions. Then, we apply a kinetic model to calculate the rates for each geometric configuration (defined by a single intermolecular direction, orientation, and distance) where the process may occur. Because this procedure must be repeated few hundreds of times and we are aiming at a model to be

applied to realistic photosensitizers, we should care that computational costs are kept under reasonable limits. To keep the computational costs under control, we seek 1) to minimize the number of quantum-chemical calculations required, 2) to replace calculations on the monomers for those on the complex whenever possible, and 3) to apply the simplest kinetic model valid for the system in hand.

The theory of nonadiabatic reaction rates for weakly-coupled systems has been developed within the Harvey-Aschi approach,⁹ which has been applied to treat unimolecular and small bimolecular systems.¹⁰ Although it could be, in principle, applied here, to determine state densities, minimum energy crossing points, and hopping probabilities for each geometric configuration would be computationally prohibitive. For this reason, we have looked for more affordable alternatives. In many situations, a nonadiabatic process, taking place either conserving the spin multiplicity (internal conversion, IC) or not (intersystem crossing, ISC) may be formulated in terms of inverted Marcus theory, as two diabatic parabolic potentials crossing at a certain point (Figure 1(a)). This situation is exactly what we expect to happen in the intersystem crossing of $^3\text{PS} \rightarrow ^1\text{PS}$ or the internal conversion of $^1[^3\text{PS}+^3\text{O}_2] \rightarrow ^1[^1\text{PS}+^1\text{O}_2]$ (reaction (1)). To investigate the nonadiabatic process, both the coupling (spin-orbit coupling for ISC, diabatic couplings for IC) and the energy gap between the relevant states should be considered. The coordinate \mathbf{R} , defining the parabolic potential, is a general set of coordinates promoting the crossing of the two states. As \mathbf{D} has a minor

contribution to the state crossing, the reaction effectively takes place not on the parabolic potentials of Figure 1(a), but on the parabolic sheets of Figure 1(b).

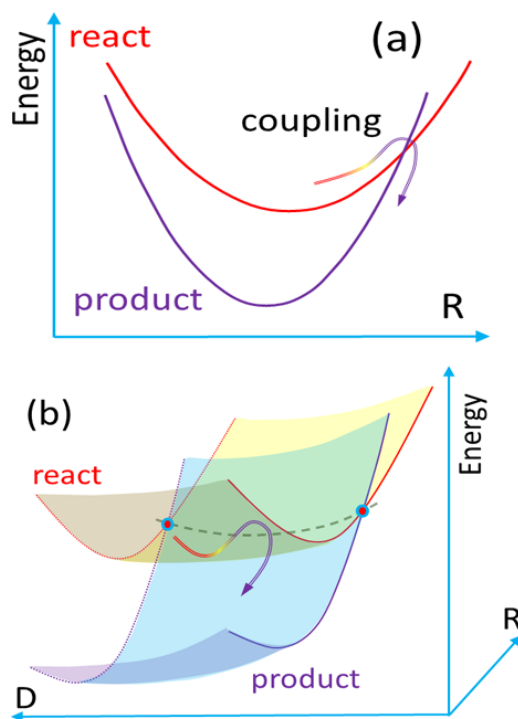


Figure 1. (a) Inverted Marcus model for energy transfer along \mathbf{R} . (b) Extension of the inverted Marcus model along the intramolecular (tuning) coordinate \mathbf{D} , and intermolecular (crossing) coordinate \mathbf{R} .

With the goal of getting rates for energy transfer for such floppy and weakly-coupled complexes, we have built a kinetic model, where all quantities needed for computing the rate in a Marcus-type model—the activation energy, the reorganization energy, and the diabatic coupling—are calculated in orthogonal segments in the \mathbf{D} - \mathbf{R} space. The motivation for such a splitting comes from the different strengths of the interactions (valence bonds in \mathbf{R} versus van de Waals interactions along \mathbf{D}), which lend these two

sets of coordinates different roles in the reaction. Aiming at keeping the computational costs at the operable level, the model still explores the **D-R** space, to minimize the number of computations done on the complex itself, replacing them, whenever possible, by computations on the isolated monomers. This strategy of splitting the calculations into orthogonal segments in the **D-R** space has inspired the name of the model, Divide-to-Conquer.

As a test case, the Divide-to-Conquer model is applied to the reaction of O₂ with the photosensitizer 6-aza-2-thiothymine (6n-2tThy). This choice is motivated by the relatively large singlet oxygen yield of 6n-2tThy (0.69 according to Ref.¹¹) and by the fact that this molecule has been subjected to several experimental and theoretical studies,^{5, 11-12} providing a reliable benchmark for testing our results. To put it in context, the development of the Divide-to-Conquer model has been part of a long research program on the properties of thiothymines. We started with the spectroscopic characterization of these molecules,^{4d} then, we modeled their triplet-state intrinsic decay.⁵ Now, we present the development of the kinetic model for energy transfer, and, finally, the analysis of the complete oxygen-generation process will be discussed in a next work.

2 Method description

2.1 Semiclassical kinetic model for energy-transfer rate

The singlet oxygen photosensitization is a typical weak-coupling energy-transfer problem, for which the Fermi's Golden rule is an excellent starting point to describe its rate:⁷

$$k_{ij} = \frac{2\pi}{\hbar} |V_{ij}|^2 \rho(E_j)_{E_j \approx E_i}. \quad (2)$$

For a radiationless process, V_{ij} is the diabatic coupling between states i and j with energies E_i and E_j , while ρ is the density of crossing states. The computation of this density has been effectively developed for unimolecular and bimolecular chemical reactions in previous works (see Ref.¹³ and references therein), but for intermolecular energy transfer in floppy complexes, this quantity still requires cumbersome approaches to be obtained.^{7a, 7b, 14} This difficulty motivates to take the classical limit of Eqn. (2),^{7c, 8a} which in the harmonic approximation is reduced to the Marcus expression:^{14a}

$$k_{ij} = \frac{2\pi}{\hbar} |V_{ij}|^2 \frac{1}{\sqrt{4\pi\lambda k_B T}} \exp\left(-\frac{(\Delta G^0 + \lambda)^2}{4\lambda k_B T}\right), \quad (3)$$

where λ is the reorganization energy and ΔG^0 is the total Gibbs free energy change for the reaction. The classical limit in Eqn. (3) is rigorously valid only if the frequencies defining the Marcus parabolic potentials are much smaller than the thermal energy $k_B T$ (i.e., 200 cm⁻¹ for 300 K). This is the case for 6n-2tThy, whose relevant harmonic normal

mode of the T_1 state is only 62 cm^{-1} (see electronic supporting information, ESI, S1). For the low temperature limit, see ref. ^{14b}

The argument of the exponential in Eqn. (3) is simply $-\Delta G^\ddagger/k_B T$, where ΔG^\ddagger is the free activation energy to reach the crossing point between the two diabatic states. In the routine formulation of Marcus theory, aimed at the electron-transfer problem, it is supposed that free energy curves of reactants and products share the same harmonic frequency so that the activation free energy can be computed from ΔG^0 and λ , as given in the exponential term of Eqn. (3). However, this approximation may not always work well, especially for energy-transfer problems, where the electronic states of reactants and products may have significantly different free energy curves. A simple workaround is available when the coupling between the states depends mostly on the internal coordinates of the monomers (or the inner shell, in Marcus theory language). In such a case, ΔG^\ddagger can be simply obtained by directly optimizing the crossing point of the monomer. This treatment has been used and proved to work well for the analysis of ISC processes in ref.⁵

For energy-transfer problems, which take place in the inverted Marcus region, reactants and products share nearly the same molecular structure (see Figure 1(a)). Therefore, enthalpic and entropic variations are small and the free energy difference is close to the potential energy difference. (Previous experimental work has confirmed that the entropy variation is near to zero for energy transfer between rigid molecules.¹⁵)

For this reason and to simplify the calculations, we have taken the activation energy ΔE^\ddagger , rather than ΔG^\ddagger , to compute the rate. (The implication of this approximation is discussed in Section 2.5.) Thus, the following equation is used for the rate calculation:

$$k_{ij} = \frac{2\pi}{\hbar} |V_{ij}|^2 \frac{1}{\sqrt{4\pi\lambda k_B T}} \exp\left(-\frac{\Delta E^\ddagger}{k_B T}\right). \quad (4)$$

To calculate the rate in Eqn. (4), we must obtain the activation energy ΔE^\ddagger , the reorganization energy λ , and the diabatic coupling V_{ij} . The calculation of the energies is discussed in Section 2.2. The coupling computation is the subject of Section 2.3.

2.2 Energies of the PS-O₂ complex

As mentioned in the Introduction, we treat the complex by dividing it coordinate subsets. Given a certain relative orientation between the PS and O₂, the complex can be described regarding three sets of coordinates: \mathbf{R} , the internal coordinates of PS; \mathbf{r} , the internal coordinates of O₂; and \mathbf{D} , the vector connecting the two monomers. As indicated in reaction (1), for the singlet oxygen photosensitization problem, the complex is initially prepared in a singlet state of the complex, which couples both PS and O₂ in their triplet states. Throughout this paper, this state is indicated by the notation $^1(\text{TT})$. (More generally, $^M(IJ)$ will indicate an arbitrary state of the complex in term of the states I and J of the monomers coupled with multiplicity M .)

We suppose that PS and O₂ are initially far away from each other. At this initial distance D , PS and O₂ behave as isolated monomers with geometries \mathbf{R}_0 and \mathbf{r}_0 of the

minimum of their triplet states. Thus, initially, the energy of the complex is just the sum of the monomers' energies, and the diabatic coupling is zero.

The adiabatic energy $E_{IJ}^{PS-O2}(\mathbf{R}, \mathbf{r}, \mathbf{D})$ of the complex at the geometry $(\mathbf{R}, \mathbf{r}, \mathbf{D})$ and state ${}^1(IJ)$ can be decomposed as a sum of the monomers' energies E_I^{PS} and E_J^{O2} plus their interaction energy U_{IJ}^{PS-O2} :

$$E_{IJ}^{PS-O2}(\mathbf{R}, \mathbf{r}, \mathbf{D}) = E_I^{PS}(\mathbf{R}) + E_J^{O2}(\mathbf{r}) + U_{IJ}^{PS-O2}(\mathbf{R}, \mathbf{r}, \mathbf{D}) . \quad (5)$$

From the three terms on the right side of Eqn. (5), the interaction energy is the most complicated, because it depends on the three sets of coordinates. We introduce the following hypothesis to simplify the interaction energy calculation:

Hypothesis I: *The interaction energy between the monomers mainly depends on the intermolecular vector \mathbf{D} , and it approximately does not depend on their internal coordinates \mathbf{R} and \mathbf{r} .*

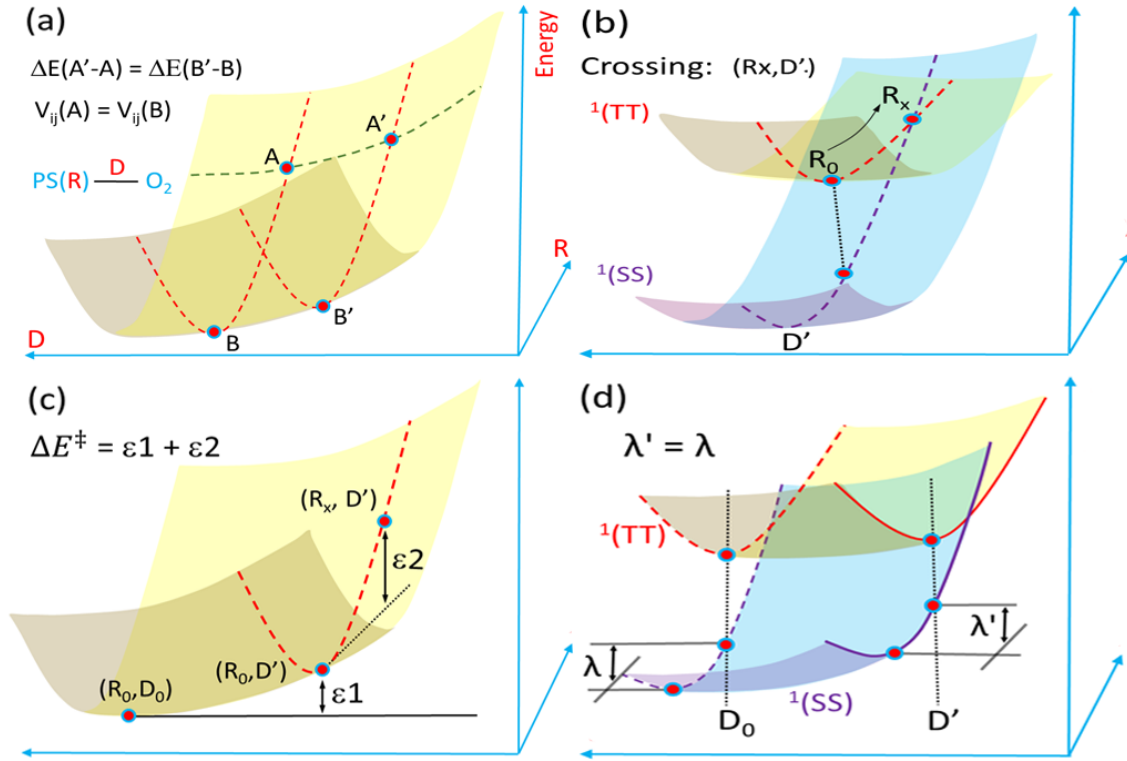


Figure 2. Schematic definition of the geometric and energetic parameters in the Divide-to-Conquer model.

Hypothesis I implies that if PS is distorted from \mathbf{R}_0 to geometry \mathbf{R}' , or O_2 is distorted from \mathbf{r}_0 to \mathbf{r}' , or both, the interaction energy does not change:

$$\begin{aligned} \Delta U_U^{PS-O_2}(\mathbf{R}_0 \rightarrow \mathbf{R}', \mathbf{r}_0, \mathbf{D}') &\equiv U_U^{PS-O_2}(\mathbf{R}', \mathbf{r}_0, \mathbf{D}) - U_U^{PS-O_2}(\mathbf{R}_0, \mathbf{r}_0, \mathbf{D}) \approx 0, \\ \Delta U_U^{PS-O_2}(\mathbf{R}_0, \mathbf{r}_0 \rightarrow \mathbf{r}', \mathbf{D}) &\equiv U_U^{PS-O_2}(\mathbf{R}_0, \mathbf{r}', \mathbf{D}) - U_U^{PS-O_2}(\mathbf{R}_0, \mathbf{r}_0, \mathbf{D}) \approx 0, \\ \Delta U_U^{PS-O_2}(\mathbf{R}_0 \rightarrow \mathbf{R}', \mathbf{r}_0 \rightarrow \mathbf{r}', \mathbf{D}) &\equiv U_U^{PS-O_2}(\mathbf{R}', \mathbf{r}', \mathbf{D}) - U_U^{PS-O_2}(\mathbf{R}_0, \mathbf{r}_0, \mathbf{D}) \approx 0, \end{aligned} \quad (6)$$

where the notation $\Delta P(\mathbf{Q} \rightarrow \mathbf{Q}')$ indicates the energy difference $\Delta P(\mathbf{Q} \rightarrow \mathbf{Q}') \equiv P(\mathbf{Q}') - P(\mathbf{Q})$. A necessary condition for this hypothesis to work well is that the character of the two states remains constant along the distortion, due to the

dependence of the interaction energy on the intermolecular orbital overlap. Later in Section 4.2, we will discuss the performance of Hypothesis I on the tested PS-O₂ system.

From Eqn. (6) and Eqn. (5), we have

$$\begin{aligned} \Delta E_{IJ}^{PS-O_2}(\mathbf{R}', \mathbf{r}', \mathbf{D}_0 \rightarrow \mathbf{D}') - \Delta E_{IJ}^{PS-O_2}(\mathbf{R}_0, \mathbf{r}_0, \mathbf{D}_0 \rightarrow \mathbf{D}') \\ = \Delta U_{IJ}^{PS-O_2}(\mathbf{R}', \mathbf{r}', \mathbf{D}_0 \rightarrow \mathbf{D}') - \Delta U_{IJ}^{PS-O_2}(\mathbf{R}_0, \mathbf{r}_0, \mathbf{D}_0 \rightarrow \mathbf{D}') \quad (7) \\ \approx 0. \end{aligned}$$

Therefore, the energy difference along the state ¹(*IJ*) when the distance between the monomers is shifted from \mathbf{D}_0 to \mathbf{D}' does not depend on the internal geometry of the monomers:

$$\Delta E_{IJ}^{PS-O_2}(\mathbf{R}', \mathbf{r}', \mathbf{D}_0 \rightarrow \mathbf{D}') \approx \Delta E_{IJ}^{PS-O_2}(\mathbf{R}_0, \mathbf{r}_0, \mathbf{D}_0 \rightarrow \mathbf{D}'). \quad (8)$$

This relationship, which is illustrated in Figure 2(a), means that the energy differences can be simply computed from the monomers' original geometries.

2.2.1 Determination of the crossing structure \mathbf{R}_x

Given a certain D' distance along a specific direction \mathbf{D} , to calculate the activation energy, we need to determine the structure of the monomers ($\mathbf{R}_x, \mathbf{r}_x$), which causes a crossing between the ¹(TT) and ¹(SS) states of the PS-O₂ complex. (The ¹(SS) state is the target singlet state of the complex, whose monomers are individually in the singlet state too.) The procedure to determine this crossing structure is discussed in this subsection.

For O₂, the only internal dimension is the distance between the two atoms, and the energy difference between the ³ Σ_g^- state and either ¹ Δ_g or ¹ Σ_g^+ states does not change much along this dimension. Therefore, the contribution of O₂ distortion to the crossing

point can be neglected, which means that we assume \mathbf{r}_x is always \mathbf{r}_0 . This assumption will simplify the calculation for PS-O₂, but it is worth noting that for a general system with two large molecules, a similar treatment could also be applied, considering both molecules.

To determine the crossing structure \mathbf{R}_x of PS, we start from the energy decomposition in Eqn. (5). The energy gap between the ¹(TT) and ¹(SS) states is

$$\begin{aligned}\Delta E_{TT-SS}^{PS-O_2}(\mathbf{R}, \mathbf{r}, \mathbf{D}') &\equiv E_{TT}^{PS-O_2}(\mathbf{R}, \mathbf{r}, \mathbf{D}') - E_{SS}^{PS-O_2}(\mathbf{R}, \mathbf{r}, \mathbf{D}') \\ &= \Delta E_{T-S}^{PS}(\mathbf{R}) + \Delta E_{T-S}^{O_2}(\mathbf{r}) + \Delta U_{TT-SS}^{PS-O_2}(\mathbf{R}, \mathbf{r}, \mathbf{D}'),\end{aligned}\quad (9)$$

where

$$\begin{aligned}\Delta E_{T-S}^{PS} &\equiv E_T^{PS} - E_S^{PS}, \\ \Delta U_{TT-SS}^{PS-O_2} &\equiv U_{TT}^{PS-O_2} - U_{SS}^{PS-O_2}.\end{aligned}\quad (10)$$

By definition, at the crossing point $(\mathbf{R}_x, \mathbf{r}_0, \mathbf{D}')$

$$\Delta E_{TT-SS}^{PS-O_2}(\mathbf{R}_x, \mathbf{r}_0, \mathbf{D}') = 0. \quad (11)$$

As a consequence of Hypothesis I, the following approximation is valid:

$$\Delta U_{TT-SS}^{PS-O_2}(\mathbf{R}_x, \mathbf{r}_0, \mathbf{D}') \approx \Delta U_{TT-SS}^{PS-O_2}(\mathbf{R}_0, \mathbf{r}_0, \mathbf{D}'). \quad (12)$$

Inserting Eqns. (9) and (12) into (11) results in

$$\begin{aligned}0 &= \Delta E_{T-S}^{PS}(\mathbf{R}_x) + \Delta E_{T-S}^{O_2}(\mathbf{r}_0) + \Delta U_{TT-SS}^{PS-O_2}(\mathbf{R}_0, \mathbf{r}_0, \mathbf{D}') \\ &= \Delta E_{T-S}^{PS}(\mathbf{R}_x) - \Delta E_{T-S}^{PS}(\mathbf{R}_0) \\ &\quad + \left[\Delta E_{T-S}^{PS}(\mathbf{R}_0) + \Delta E_{T-S}^{O_2}(\mathbf{r}_0) + \Delta U_{TT-SS}^{PS-O_2}(\mathbf{R}_0, \mathbf{r}_0, \mathbf{D}') \right] \\ &= \left(\Delta E_{T-S}^{PS}(\mathbf{R}_x) - \Delta E_{T-S}^{PS}(\mathbf{R}_0) \right) + \Delta E_{TT-SS}^{PS-O_2}(\mathbf{R}_0, \mathbf{r}_0, \mathbf{D}').\end{aligned}\quad (13)$$

This result shows that for the energy gap of the complex, the terms determined by either \mathbf{R} or \mathbf{D} can be calculated separately, and the sum of them should be zero for the crossing point. This relationship is illustrated in Figure 2(b).

From Eqn. (13), we get our final result in this subsection:

$$\Delta E_{T-S}^{PS}(\mathbf{R}_x) = \Delta E_{T-S}^{PS}(\mathbf{R}_0) - \Delta E_{TT-SS}^{PS-O2}(\mathbf{R}_0, \mathbf{r}_0, \mathbf{D}'). \quad (14)$$

Eqn. (14) can be used to determine \mathbf{R}_x . In practice, we first compute the reaction pathway between \mathbf{R}_0 and the triplet-singlet crossing point \mathbf{R}_{isc} for PS. This can be done with the optimized structures from the quantum chemical calculation, for instance by linear interpolation of internal coordinates (LIIC). Then, we determine the point \mathbf{R}_x in this reaction pathway to be the point where the triplet-singlet energy gap $\Delta E_{T-S}^{PS}(\mathbf{R}_x)$ has the values as calculated in Eqn. (14) for a certain \mathbf{D}' . With this result, we have the crossing point as a specific geometry labeled $(\mathbf{R}_x, \mathbf{r}_0, \mathbf{D}')$, and calculate the final activation energy as explained in the next subsection.

2.2.2 Computation of the activation energy ΔE^\ddagger

The complex is initially prepared in the state $^1(TT)$ with geometry $(\mathbf{R}_0, \mathbf{r}_0, \mathbf{D}_0)$ and the top of the conversion barrier for an arbitrary inter-monomer distance D' is at $(\mathbf{R}_x, \mathbf{r}_0, \mathbf{D}')$, as discussed in Subsection 2.2.1. Then, the activation energy will be

$$\Delta E^\ddagger(\mathbf{D}') = E_{TT}^{PS-O2}(\mathbf{R}_x, \mathbf{r}_0, \mathbf{D}') - E_{TT}^{PS-O2}(\mathbf{R}_0, \mathbf{r}_0, \mathbf{D}_0). \quad (15)$$

This equation can still be rewritten as

$$\begin{aligned} \Delta E^\ddagger(\mathbf{D}') = & \left[E_{TT}^{PS-O_2}(\mathbf{R}_x, \mathbf{r}_0, \mathbf{D}') - E_{TT}^{PS-O_2}(\mathbf{R}_0, \mathbf{r}_0, \mathbf{D}') \right] \\ & + \left[E_{TT}^{PS-O_2}(\mathbf{R}_0, \mathbf{r}_0, \mathbf{D}') - E_{TT}^{PS-O_2}(\mathbf{R}_0, \mathbf{r}_0, \mathbf{D}_0) \right]. \end{aligned} \quad (16)$$

Inserting Eqn. (5) into (16) and taking into account that both monomers are in the triplet state T we have

$$\begin{aligned} \Delta E^\ddagger(\mathbf{D}') = & \Delta E_T^{PS}(\mathbf{R}_0 \rightarrow \mathbf{R}_x) + \Delta U_{TT}^{PS-O_2}(\mathbf{R}_0 \rightarrow \mathbf{R}_x, \mathbf{r}_0, \mathbf{D}') \\ & + \Delta U_{TT}^{PS-O_2}(\mathbf{R}_0, \mathbf{r}_0, \mathbf{D}_0 \rightarrow \mathbf{D}'). \end{aligned} \quad (17)$$

With Eqn. (17), the calculation of the complex energies is simplified because each interaction term on the right side depends on changes on a single coordinate, either \mathbf{R} or \mathbf{D} . Using Eqns. (5) and (7) under Hypothesis I, the final formula for the activation energy is:

$$\begin{aligned} \Delta E^\ddagger(\mathbf{D}') \approx & \Delta E_T^{PS}(\mathbf{R}_0 \rightarrow \mathbf{R}_x) + \Delta E_T^{PS-O_2}(\mathbf{R}_0, \mathbf{r}_0, \mathbf{D}_0 \rightarrow \mathbf{D}') \\ = & \varepsilon 1 + \varepsilon 2. \end{aligned} \quad (18)$$

In Eqn. (18), $\varepsilon 1 \equiv \Delta E_T^{PS}(\mathbf{R}_0 \rightarrow \mathbf{R}_x)$ is computed for the isolated PS monomer, while $\varepsilon 2 \equiv \Delta E_J^{AB}(\mathbf{R}_0, \mathbf{r}_0, \mathbf{D}_0 \rightarrow \mathbf{D}')$ is computed for the complex at frozen internal geometries $(\mathbf{R}_0, \mathbf{r}_0)$ for two intramolecular distances, D_0 and D' . These quantities are illustrated in Figure 2(c). Note yet that for a general system where larger molecule replaces O_2 , a similar treatment still holds, but with the activation energy containing three terms instead of two.

2.2.3 Reorganization energy λ

The next element missing for the computation of the energy-transfer rate in Eqn. (4) is the reorganization energy λ . As shown in Eqn. (4) and discussed before,^{7c} the rate

does not depend on λ as much as it depends on the diabatic coupling and the activation energy. Thus, λ can be calculated under stronger approximations.

The reorganization energy λ , usually divided into internal and outer parts, accounts for the nuclear distortions along the Marcus parabolic potentials.¹⁶ For internal conversion, the internal coordinates of the monomer dominate these nuclear distortions, meaning that the outer part due to solvent relaxation may be ignored. With the focus on the inner part, we need the minimum structures for the initial and final states of the monomers. For the two states, the minimum structure of PS changes much more than that of O₂, because the triplet ground state and singlet excited states of O₂ share the same molecular orbitals. Therefore, for a certain \mathbf{D}' , the state energy of PS-O₂ should be mainly determined by the internal motion of PS, and we take its minimum structures of the T₁ and S₀ states with frozen O₂ as an approximation for the minimum structure energies of the complex.

According to its definition and once more neglecting enthalpic and entropic effects, λ should be calculated as

$$\lambda = E_J(\mathbf{R}_0, \mathbf{r}_0, \mathbf{D}') - E_J(\mathbf{R}'_0, \mathbf{r}_0, \mathbf{D}'). \quad (19)$$

In this equation, $(\mathbf{R}_0, \mathbf{r}_0, \mathbf{D}')$ is the minimum of the ¹(TT) state, as used in the previous sections, while $(\mathbf{R}'_0, \mathbf{r}_0, \mathbf{D}')$ is the minimum of the ¹(SS) state. Using Eqn. (5) and Hypothesis I, Eqn. (19) can be written as

$$\begin{aligned}\lambda &= \Delta E_{TT}^{PS}(\mathbf{R}_0 \rightarrow \mathbf{R}'_0) + \Delta U_{TT}^{PS-O_2}(\mathbf{R}_0 \rightarrow \mathbf{R}'_0, \mathbf{r}_0, D') \\ &\approx \Delta E_{TT}^{PS}(\mathbf{R}_0 \rightarrow \mathbf{R}'_0).\end{aligned}\tag{20}$$

Eqn. (20) implies that the reorganization energy of the PS-O₂ complex is very close to the one of PS itself. This result can be understood from the physical meaning of reorganization energy: the reorganization energy originates from the effect of vibrational nuclear motion to reach the new equilibrium geometry of the final state. In the oxygen molecule, the ground triplet state and the first two singlet states share the same geometry within 0.02 Å.¹⁷ Therefore, for a certain intermolecular distance, most of the nuclear relaxation comes from the vibrational motion of PS motion, with little or no contribution from O₂. This treatment of the reorganization energy is illustrated in Figure 2(d).

2.3 Calculation of Diabatic Coupling

The last missing element we need to compute the rate in Eqn. (4) is the diabatic coupling V_{ij} . There is a large variety of methods to compute diabatic Hamiltonian matrices,¹⁸ from which diabatic couplings are the nondiagonal elements. Diabatic couplings computed with any of such methods may be plugged in Eqn. (4). Given that diabatic couplings are not a quantity commonly available in most of the computational chemistry packages, we outline here the method used in this work. We stress, however, that it is not part of the Divide-to-Conquer model, as any other approach could have been used.

Diabatic couplings can be computed from adiabatic states through an adiabatic to diabatic transformation.¹⁹ This transformation can be based on different approaches, including methods working on nonadiabatic couplings, energies, or other properties. For the problem in hand, singlet oxygen generation, we must deal with open shell states. For this reason, we decided to work with multiconfigurational wave functions, as discussed later. Because for such methods there are efficient algorithms to compute nonadiabatic couplings analytically,²⁰ we have chosen to calculate the diabatic couplings using a nonadiabatic-coupling-based method.

As a first approximation, we supposed that only diabatic couplings between $^1(\text{TT})$ and each of the $^1(\text{SS})$ states are relevant and that diabatic couplings between $^1(\text{SS})$ states could be neglected. This simplifies the problem to a set of uncoupled two-states adiabatic-to-diabatic transformations.²¹ These transformations are unitary, corresponding to a rotation in a 2D plane by an angle θ given by¹⁹

$$\nabla\theta = \mathbf{F}_{ij} \equiv \langle \psi_i | \nabla | \psi_j \rangle, \quad (21)$$

where \mathbf{F}_{ij} is the nonadiabatic coupling vector between the adiabatic states with wave functions ψ_i and ψ_j .

As usual for nonadiabatic-coupling-based methods, we assume that the coupling depends on a 1D path,²² in our case defined by the intramolecular vector \mathbf{D} . This approximation turns Eqn. (21) into a 1D problem

$$\frac{d\theta}{dD} = \mathbf{F}_{ij}^D, \quad (22)$$

where \mathbf{F}_{ij}^D is the projection of the nonadiabatic coupling vector on the direction \mathbf{D} . Eqn.

(22) can be simply integrated by finite differences, as long as we have 1) an initial value for θ (we took $\theta(D_0) = 0$) and 2) the values of \mathbf{F}_{ij} as a function of D .

After getting $\theta(D)$, the diabatic coupling can be simply computed as (ESI, S2)

$$V_{ij}(D) = \frac{\Delta E_{ij}(D) \sin(2\theta(D))}{2}, \quad (23)$$

where ΔE_{ij} is the adiabatic energy gap between states i and j .

2.4 Divider-to-Conquer in a nutshell

Supposing an internal conversion problem of the type ${}^1(\text{TT}) \rightarrow {}^1(\text{SS})$, the main steps to apply the Divide-to-Conquer model are:

1. For the isolated PS, compute the minimum of the triplet state \mathbf{R}_0 , the intersystem crossing point \mathbf{R}_{isc} (between the singlet and the triplet state of PS), and the potential energy profile between these two geometries.
2. Choose an initial relative orientation between PS and O_2 , and compute the potential energy profile for the PS- O_2 complex along \mathbf{D} at fixed \mathbf{R}_0 and \mathbf{r}_0 .
3. Use Eqn. (14) to determine \mathbf{R}_x .
4. Compute the activation energy ΔE^\ddagger with Eqn. (18).
5. With the energies of the isolated PS, compute the reorganization energy λ with Eqn. (20).

6. Compute the diabatic coupling V_{ij} along \mathbf{D} for fixed \mathbf{R}_0 and \mathbf{r}_0 . If only nonadiabatic couplings are available, use the method outlined in Section 2.3 (see below).
7. Compute the reaction rate along \mathbf{D} with Eqn. (4).

The main geometrical and energetic parameters for these calculations are indicated in Figure 2. Steps 1 to 7 may be repeated starting from all relative orientations of interest.

If diabatic couplings are to be computed with the method discussed in Section 2.3:

1. Compute nonadiabatic couplings vectors \mathbf{F}_{ij} along \mathbf{D} for fixed \mathbf{R}_0 and \mathbf{r}_0 .
2. Integrate Eqn. (22) numerically to obtain $\theta(D)$.
3. Compute $V_{ij}(D)$ with Eqn. (23).

2.5 Limitations of the model

In this first version, the Divide-to-Conquer model has few limitations we should be aware of. First, it does not account for entropic and enthalpic effects in the activation and reorganization energies. Although these effects tend to cancel out in an inverted-Marcus type of problem, small uncertainties in the activation energy may still have large consequences for the rate, due to the exponential dependence of the latter on the former. For this reason, it may be a good policy to focus the analysis on relative, rather than on absolute rate values. The extension of the model to include entropic and enthalpic corrections is in principle trivial, albeit computationally demanding. In doing that, rates should be computed still with Eqn. (4), but with ΔE^\ddagger replaced by ΔG^\ddagger .

The second limitation is that the relative rotation of the monomers is not accounted for, as the model assumes a rigid radial approach between them. The major impact of this approximation should be on the diabatic coupling, which should depend on the relative orientation of the monomers. This dependence is evident, for instance, when diabatic couplings are integrated from nonadiabatic couplings (Eqn. (21)). The integration is done over a predefined path, which here was taken to be the rigid radial approach. This neglecting of rotation should affect the rate less significantly, than any error in the activation energy, given the functional dependencies in Eqn. (4).

A third limitation is an implicit assumption that the vibrational frequency associated with \mathbf{R} is much smaller than the thermal energy. As mentioned, this approximation is essential to reduce the problem to a simple Marcus-type formulation. If it does not hold, more involved kinetic formulation, with explicit computation of the density of states may be needed.^{10, 23} Note that this is not a limitation of the Divide-to-Conquer model, which can still be applied using this alternative kinetic formulation.

A final limitation, the use of Hypothesis I, is discussed in Section 4.2.

3 Computational Details

Geometry optimizations and excited states of 6n-2tThy and O₂ as isolated molecules were computed with the complete active space perturbation theory to the second order (CASPT2) in its multi-state (MS) version.²⁴ For 6n-2tThy the active space is composed of 10 electrons in 7 orbitals (10,7), the same that we have used and tested in previous

work⁵ (see also ESI, S3). For O₂, the space is (6,6). For both molecules, we used the ANO-RCC-VTZP basis set. Standard IPEA (0.25 a.u.)²⁵ was globally adopted in the CASPT2 calculations, and no level shift was employed. All these calculations were done with Molcas 8.²⁴ Cartesian coordinates for the optimized structures are given in the ESI (S4).

The calculations of the PS-O₂ complex, including the excited energies and nonadiabatic coupling vectors (NAC) along the **D** direction were done at the complete active space self-consistent field level with 12 electrons in 9 orbitals (CASSCF(12,9)). In this active space, a (6,4) subspace described the oxygen molecule. The CASSCF calculations were done with the 6-31G** basis set, using the COLUMBUS software.²⁶

Two **D** directions were investigated here, both with the O₂ oriented perpendicular to 6n-2tThy. In the first one, named “to-56 direction,” the vector was defined along as $\mathbf{D}_{\text{to-56}} = (\mathbf{Q}_{C5}^{PS} + \mathbf{Q}_{N6}^{PS}) / 2 - \mathbf{Q}^{O2}$, where \mathbf{Q}_{C5}^{PS} and \mathbf{Q}_{N6}^{PS} are the position of atoms C5 and N6 of PS, and \mathbf{Q}^{O2} is the position of the nearest oxygen atom in O₂. In the second direction, named “to-N3,” the vector was $\mathbf{D}_{\text{to-N3}} = \mathbf{Q}_{N3}^{PS} - \mathbf{Q}^{O2}$, where \mathbf{Q}_{N3}^{PS} is the position of N3. In the figures, the intermolecular distances for to-56 direction are defined as $D_{\text{to-56}} = |\mathbf{Q}_{N6}^{PS} - \mathbf{Q}^{O2}|$ and for the to-N3 direction, $D_{\text{to-N3}} = |\mathbf{D}_{\text{to-N3}}|$. In both cases, the initial distance D_0 was taken as approximately $1.5R_O + R_N$, where R_O and R_N are the van der Waals radii of oxygen and nitrogen, i.e. about 3.9 Å.

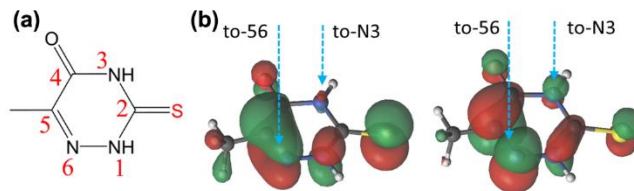


Figure 3. (a) Structure and numbering of 6-aza-2-thiothymine (6n-2tThy); (b) Singly-occupied orbitals of the T_1 state of 6n-2tThy at the T_1 minimum. The two investigated incidence directions of the O_2 are indicated by arrows.

4 Results and Discussion

4.1 Energies and nonadiabatic couplings

The purpose of the calculations is to test the Divide-to-Conquer model on the singlet oxygen photosensitized by 6n-2tThy. To generate singlet oxygen starting from this PS, internal conversion from the PS- O_2 state $^1(TT)$ to either $^1(SS)_2$, $^1(SS)_1$, or $^1(SS)_0$ state should take place (reaction (1)). We will investigate rates for this reaction for two different incidence/orientation directions, which we have chosen motivated by the results for the T_1 state of 6n-2tThy discussed in ref.⁵

The structure and numbering of 6n-2tThy are shown in Figure 3(a). In the first incidence/orientation direction, the O_2 approaches perpendicularly to the middle of C5-N6 bond on PS (see Figure 3(b) and Figure 4(a)). Along this direction—we call it the “to-56” direction, there is a large overlap between the electronic density of O_2 and the exciton in 6n-2tThy. In the second incidence/orientation direction, the O_2 approaches PS perpendicularly to N3 (Figure 3(b) and Figure 4(b)). Along this “to-N3” direction, the O_2 -PS excitonic overlap is near to zero. Based only on the difference

between these overlaps, we may already expect that the reaction rate along the to-56 direction should be larger than along the to-N3 direction.

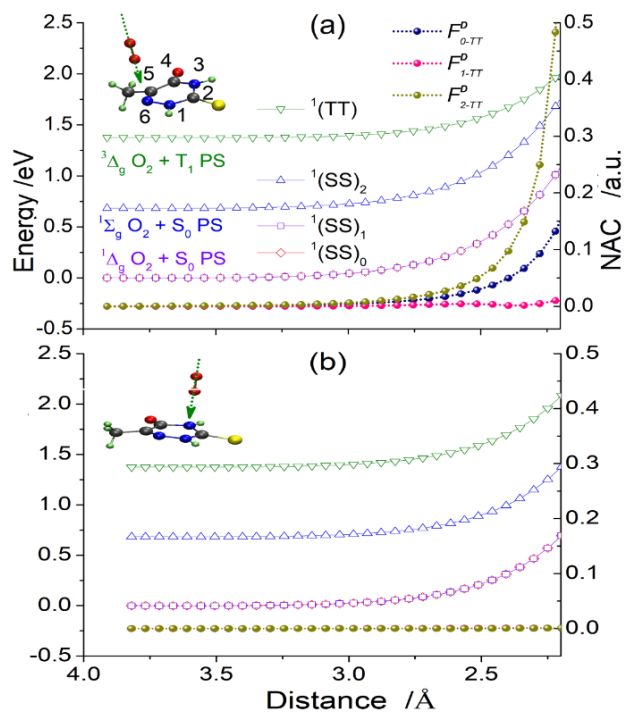


Figure 4. Excited-state energies and NAC of PS-O₂ at different distances with (a) the to-56 direction and (b) to-N3 direction. The green arrows show the direction of \mathbf{D} . $F_{i-\text{TT}}^{\mathbf{D}}$ is the NAC between states ${}^1(\text{TT})$ and ${}^1(\text{SS})_i$ projected on \mathbf{D} . In both graphs, the ${}^1(\text{SS})_0$ and ${}^1(\text{SS})_1$ energies are degenerated. In (b), all three NAC projections are near zero.

The potential energies of the ${}^1(\text{TT})$ and the three ${}^1(\text{SS})$ states along the two directions are shown in Figure 4. This figure also illustrates the projection of the NAC along each direction. For both directions, the potential energies start to increase due to the PS-O₂ interaction for distances D shorter than 3 Å. Along the to-56 direction, the ${}^1(\text{TT})/{}^1(\text{SS})_2$ and ${}^1(\text{TT})/{}^1(\text{SS})_1$ NACs ($F_{2-\text{TT}}^D$ and $F_{1-\text{TT}}^D$, respectively) also increase at short distances,

especially below 2.5 Å. The ${}^1(\text{TT})/{}^1(\text{SS})_0$ NAC ($F_{0-\text{TT}}^D$), however, is always near zero. Along the to-N3 direction, the NAC of the ${}^1(\text{TT})$ with all ${}^1(\text{SS})$ states is always near zero. These results for the NAC behavior along the two directions support our expectation that the rate should be larger along the to-56 than along the to-N3 direction.

4.2 Verification of Hypothesis I

As discussed in Section 2.2, Hypothesis I plays a significant role on the derivation of the Divide-to-Conquer model, stating that the interaction term of the state energy depends only on the distance D . Although this hypothesis is chemically sound, giving its importance for the model, before continuing with the calculation of the rates, we will first check its validity here. For this purpose, we need to show that the interaction term in Eqn. (5) mainly depends on the distance D . This can be done by checking the performance of Eqn. (6) in the calculations of a real system, the 6n-2tThy studied here. If Hypothesis I is valid, the potential energy curves for PS along two arbitrary values of \mathbf{R} should be parallel to the curves of the PS-O₂ complex along the same \mathbf{R} distortion at fixed D .

Through linear interpolation of internal coordinates, we connected \mathbf{R}_0 , the PS-optimized T₁ minimum, to \mathbf{R}_{isc} , the T₁/S₀ ISC structure of 6n-2tThy, to generate multiple \mathbf{R} points. Then, we calculated the S₀ and T₁ state energies of PS at these points at the CASSCF level, with the same basis set and active space as used for PS-O₂. Next, we calculated the state energies of PS-O₂ along the inner coordinates \mathbf{R} of PS and compared

them to the ones of PS with the same state character. The PS-O₂ curves were computed with D fixed at the value that maximizes the reaction rate, shown later in Subsection 4.4 to be 2.81 Å for the to-56 direction and 3.03 Å for the to-N3 direction. The results of these calculations are shown in Figure 5.

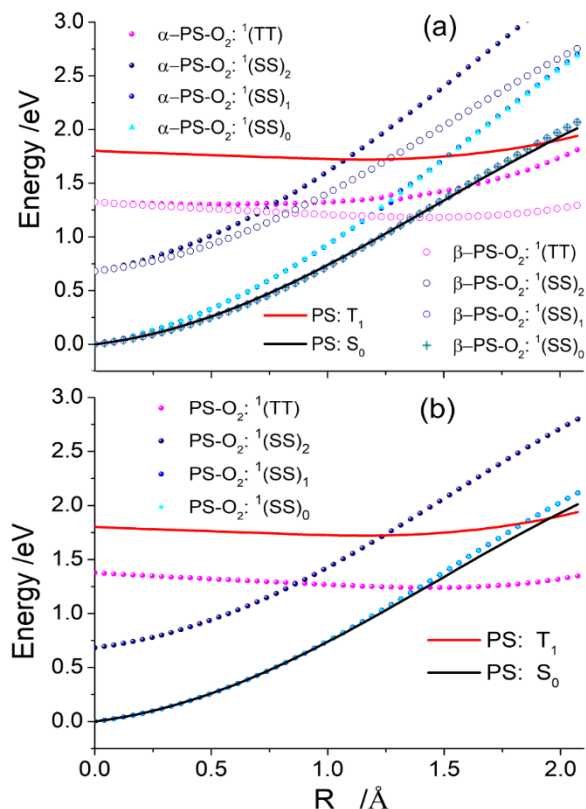


Figure 5. Comparison of the state energy of 6n-2tThy and 6n2tThy-O₂ for (a) to-56 direction and (b) to-N3 direction along \mathbf{R} . For the former, the geometry of the complex is determined in two ways: (α) fixed O₂ with 2.81 Å distance at first point, and (β) slight adjusted O₂ to keep the same distance, as explained in the text. For the to-N3 direction, only the first case with 3.03 Å distance at first point is considered. Distances are defined in Section 3.

We start the analysis with the results for the to-N3 orientation in Figure 5(b). As expected from Hypothesis I, for the same state character, the state energies of PS-O₂

are parallel to the ones of PS alone for the all values of \mathbf{R} . This result clearly shows that, in this case, the state energy of the complex along \mathbf{R} is mainly determined by the energy of PS, and the interaction term U^{PS-O_2} is nearly constant as stated by Hypothesis I. We can rephrase it by saying that the PS-O₂ interaction term is mainly determined by the distance D and not by the internal PS coordinates \mathbf{R} .

For to-56 orientation (Figure 5(a), curves α), the validity of Hypothesis I is not as clear as for the to-N3 orientation. With fixed O₂, the state energies of PS-O₂ are clearly not parallel to the ones of PS along the \mathbf{R} .

A close examination of the PS-O₂ energy profiles shows a fundamental difference between the two orientations. While in the profile for the to-N3 orientation the N3 atom keeps nearly stationary along the \mathbf{R} distortions, in the profile for the to-56 orientation, the out-of-plane distortion of N6 along \mathbf{R} interferes with D . As a consequence, the van der Waals interaction between the monomers, which was initially supposed to depend only on the intermolecular distance, also increases with \mathbf{R} . To account for this interference, new calculations were done slightly adjusting the O₂ position along the profiles to keep the distance constant. As shown in Figure 5(a) (curves β), with such correction, the state energies of PS and PS-O₂ become parallel. This result confirms that van der Waals interactions induced by the coupling between \mathbf{D} and \mathbf{R} lead to a deviation from the assumptions in Hypothesis I.

The deviations from Hypothesis I should not affect the determination of the crossing point, which is just related to the energy gap between states. This is confirmed by the crossing points for the α and β cases in Figure 5(a), which agree with each other within 0.1 Å. Nevertheless, the calculation of activation energy may be more sensitive to deviations from Hypothesis I. In this work, we still use the Hypothesis I because of the computational simplicity, as well as due to the following reasons: a) for the main reaction contributing to the singlet oxygen generation, ${}^1(\text{TT}) \rightarrow {}^1(\text{SS})_3$, the crossing point occurs for a relatively small \mathbf{R} and the error is negligible (less than 0.1 eV); b) the to-56 direction is one of the directions with the largest couplings between \mathbf{D} and \mathbf{R} to cause the error, which means that for most of other directions Hypothesis I should perform better. Still, we should keep the potential error in the activation energy in mind, especially when accurate calculations of rate for different paths is the target. In such cases, modifications in the current model may be necessary.

4.3 Diabatic couplings

Using the method discussed in Section 2.3, we calculated the diabatic couplings between the ${}^1(\text{TT})$ and the ${}^1(\text{SS})$ states as a function of the intramolecular distance D for both directions. The results for to-56 direction are shown in Figure 6; for to-N3 direction, it is given in the ESI (S5). Along the to-56 direction, the diabatic coupling between ${}^1(\text{TT})$ and the ${}^1(\text{SS})_0$ and ${}^1(\text{SS})_2$ states increases from zero to hundreds of

wavenumbers when the PS-O₂ distance is reduced. The coupling between ¹(TT) and the ¹(SS)₁ is limited to less than 50 cm⁻¹.

These coupling values can be quantitatively confirmed by direct comparison to the adiabatic minimum energy gap. At the crossing point, the diabatic state energies are equal, and the adiabatic energy gap is $\Delta E_{ij} = 2 V_{ij}$. If we take, for instance, the crossing point between the ¹(SS)₂ and ¹(TT) states the adiabatic energy gap is 0.02 eV, which means the diabatic coupling is 0.01 eV = 80.6 cm⁻¹ (see ESI, S6). The calculated diabatic coupling is for this same pair of states is 75.6 cm⁻¹, showing an excellent agreement between the two approaches.

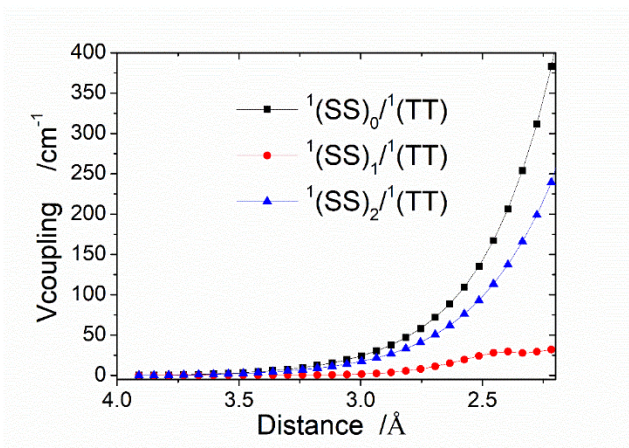


Figure 6. Diabatic coupling between state ¹(TT) and the ¹(SS) states of PS-O₂ along the to-56 direction.

4.4 Energy transfer rates

Finally, we show the energy-transfer rates for singlet oxygen generation in PS-O₂. They are given in Figure 7 for to-56 and to-N3 directions. The rates as a function of

distance have a bell shape with the maximum occurring at about 2.8 – 3.0 Å distance between PS and O₂. The maximum rates as well as the coupling, activation energy, and reorganization energy computed at the maximum are reported in Table 1.

To understand the bell shape of the rate, note that there are two competing effects. On the one hand, the closer the PS-O₂ distance, the larger the diabatic coupling (see Figure 6). On the other hand, with the O₂ approaching PS, the state energy tends to increase (Figure 4), making it hard to reach shorter PS-O₂ distances. The balance between these two trends governs the reaction rate, yielding the bell-shaped curve.

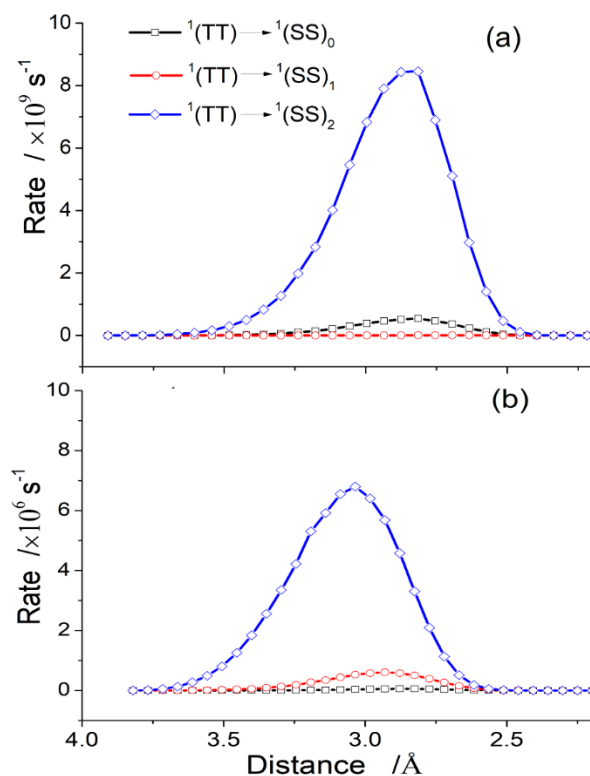


Figure 7. Energy transfer rate for singlet oxygen generation in PS-O₂ complexes along (a) the to-56 direction and (b) the to-N3 direction (PS = 6n-2tThy).

As shown in Table 1, for both directions, the rate for the transfer from the $^1(\text{TT})$ to the $^1(\text{SS})_3$ state dominates the reaction. The rates along the to-56 direction are about 1000 times larger than those along the to-N3 direction. This result is in line with our qualitative predictions based on the molecular orbital overlaps and the comparison of NACs (Section 4.1).

Table 1. PS-O₂ distance D_{max} that maximizes the rate; reorganization energy, coupling, activation energy computed at D_{max} . Maximum value of the rate and final $^1\text{O}_2$ state for both incidence/orientation directions.

to-56 direction						
	D_{max} (Å)	λ_{max} (eV)	V_{max} (cm ⁻¹)	$\Delta E_{\text{max}}^{\ddagger}$ (eV)	k_{max} (10 ⁹ s ⁻¹)	$^1\text{O}_2$ state
$^1(\text{TT}) \rightarrow ^1(\text{SS})_0$	2.81	1.34	47	0.176	0.54	$^1\Delta_g$
$^1(\text{TT}) \rightarrow ^1(\text{SS})_1$	2.69	1.34	11	0.208	0.009	$^1\Delta_g$
$^1(\text{TT}) \rightarrow ^1(\text{SS})_2$	2.81	1.34	33	0.087	8.46	$^1\Sigma_g$
to-N3 direction						
	D_{max} (Å)	λ_{max} (eV)	V_{max} (cm ⁻¹)	$\Delta E_{\text{max}}^{\ddagger}$ (eV)	k_{max} (10 ⁶ s ⁻¹)	$^1\text{O}_2$ state
$^1(\text{TT}) \rightarrow ^1(\text{SS})_0$	2.88	1.34	0.55	0.184	0.055	$^1\Delta_g$
$^1(\text{TT}) \rightarrow ^1(\text{SS})_1$	2.93	1.34	1.5	0.174	0.60	$^1\Delta_g$
$^1(\text{TT}) \rightarrow ^1(\text{SS})_2$	3.03	1.34	0.61	0.065	6.80	$^1\Sigma_g$

Singlet oxygen can be produced either in the $^1\Sigma_g$ or in the $^1\Delta_g$ state. Transition to $^1(\text{SS})_2$ will result in $^1\Sigma_g$, while the transition to either $^1(\text{SS})_0$ or $^1(\text{SS})_1$ will result in $^1\Delta_g$. As the results show, in both directions $^1\Sigma_g$ yield should exceed the $^1\Delta_g$ yield by a factor 10. The diabatic coupling for the transition to $^1(\text{SS})_0$ is larger than that to $^1(\text{SS})_2$.

Nevertheless, the smaller energy gap between $^1(\text{TT})$ and $^1(\text{SS})_2$ at \mathbf{R}_0 makes it easier to reach the crossing point with shorter displacement to \mathbf{R}_x , leading to a smaller activation energy ΔE^\ddagger and larger rate for transitions between these states.

Ref.^{3f} reports an early attempt of modeling the energy-transfer rates for weakly-bound floppy complexes in the context of singlet oxygen generation. In that work, the rates were computed directly from the Fermi's Golden Rule (Eqn. (2)), by estimating couplings from energy gaps assuming a constant density of states ρ equal to 0.1 eV^{-1} . This model was applied to complexes of O_2 with ethylene and several photosensitizers in the furocoumarin family. Their rates as a function of distance showed a systematic increase from about 10^9 to 10^{14} s^{-1} when the intramolecular distance was shrunk from 5 to 2.25 Å. This result is strongly different from ours, which is characterized by a bell shape of the rates, with a maximum rate of about 10^9 s^{-1} (see Figure 7). The reason for this divergence is mainly in the treatment of the density of states. If we take the rates computed with the Divide-to-Conquer model and use them to solve Eqn. (2) for ρ , we see that density of states is strongly dependent on the distance. We show in the ESI (S7) that, although ρ is approximately constant for distances larger than 3.3 Å, it quickly drops to zero for shorter distances. The absolute value of ρ also depends on the transitions. While for the $^1(\text{TT})_1 \rightarrow ^1(\text{SS})_2$ the density is about 0.3 eV^{-1} , it is only 0.008 eV^{-1} for $^1(\text{TT})_1 \rightarrow ^1(\text{SS})_0$ (both for $D > 3.3 \text{ Å}$).

Because of the floppy nature of the PS-O₂ complex, the reaction may take place at diverse intermolecular directions, orientations, and distances. This feature is captured by the dependence of the rate $k(\mathbf{D})$ on \mathbf{D} . Although the rate as a function of the geometry is a quantity somewhat distant from what can be experimentally measured, it has the advantage of allowing a physical understanding of the basic process, for instance indicating which electron interactions contribute the most to generate the singlet oxygen species. The rate calculated along a single direction/orientation as a function of distance is a quantitative measure of the nonadiabatic transition probability, which can be compared with the rates along other direction/orientations. In this paper, we showed results for only two of such direction/orientations, because we only aimed at presenting the method. Nevertheless, when the rates are computed over a large number of direction/orientations, they provide a basis where average rates can be computed.

Alternatively, the Dived-to-Conquer model could be linked to a nonadiabatic variational search algorithm in the spirit of the variational transition state theory (VTST).²⁷ In this case, the focus would be displaced from the rate as a function of the geometry to an effective rate. The major difficulty for such algorithm, however, would be the automatic determination of the diabatic couplings.

The rates as computed and presented here, and even their average over many directions/orientations or their variationally determined value, cannot be directly

compared to experimental rates as those reported in ref.¹¹ because they are not exactly the same quantities. While in our modelling we have approached the problem from the unimolecular standpoint (energy transfer within the complex), experimentally reported rates are defined for a bimolecular reaction.²⁸

Therefore, to make these quantities comparable, we should consider both 1) the average over energy-transfer rates obtained for all relevant incidence/orientation directions and 2) the oxygen concentration. Such collisional-theory treatment, however, would excessively elongate this work, and it will be presented in a separated paper.

5 Conclusions

In this paper, we develop a model for computing the internal conversion reaction rates for energy transfer in weakly-coupled floppy molecular complexes. The model, named Divide-to-Conquer, splits the nuclear coordinate space of the complex into orthogonal subsets of internal molecular coordinates and intermolecular distances, to minimize and simplify the amount of computation necessary to obtain activation energy, reorganization energy, and diabatic couplings. These quantities are then used to feed an inverted region Marcus-type model to provide reaction rates.

The main approximations and limitations of the model are analyzed, and possible new developments to overcome them are pointed out. All the parameters in the model are directly obtained from quantum chemical calculations for the monomers and the

complex. In our test case, this was done with MS-CASPT2 and CASSCF methods. Diabatic couplings were obtained from integration of nonadiabatic couplings computed at CASSCF level.

The Divide-to-Conquer model was applied to photosensitized singlet oxygen production in during the interaction of 6n-2tThy with O₂. This PS-O₂ test case was studied along two different incidence directions, with the O₂ hitting different regions of the 6n-2tThy photosensitizer. The results show a strong dependence of the reaction rate on the directions and states. Rates for different directions may differ by a factor 1000. Independently of direction, singlet oxygen yield in the ¹Σ_g state exceeds that in the ¹Δ_g state by a factor 10.

The Divide-to-Conquer model can be applied to other similar energy-transfer problems, especially for weakly-coupled floppy molecular complexes.

Supporting Information.

Cartesian coordinates of optimized structures; derivation of Eq. 23; vibrational mode of 6n-2tThy on T₁ state; active space for CASSCF/CASPT2 calculation; diabatic coupling for to-N3 direction; adiabatic minimum energy gap. This information is available free of charge via the Internet at <http://pubs.acs.org>.

Corresponding Authors

* SB: shuming.bai@univ-amu.fr; MB: mario.barbatti@univ-amu.fr

ORCID

Shuming Bai: 0000-0002-4993-8070

Mario Barbatti: 0000-0001-9336-6607

Notes

The authors declare no competing financial interest.

Acknowledgements

We are grateful to Prof. Hans Lischka, Prof. Troy Van Voorhis, Dr. Miquel Huix-Rotllant, and Dr. Zhou Lin for discussions and valuable suggestions. The authors thank the support of the A*MIDEX grant (n° ANR-11-IDEX-0001-02) and the project Equip@Meso (ANR-10-EQPX-29-01), both funded by the French Government “Investissements d’Avenir” program. This work was performed using HPC resources from GENCI-CINES (Grant 2017-A0010810012).

References

1. (a) Paterson, M. J.; Christiansen, O.; Jensen, F.; Ogilby, P. R., Invited review - Overview of theoretical and computational methods applied to the oxygen-organic molecule photosystem. *Photochem. Photobiol.* **2006**, *82*, 1136-1160; (b) Zhou, Z. J.; Song, J. B.; Nie, L. M.; Chen, X. Y., Reactive oxygen species generating systems meeting challenges of photodynamic cancer therapy. *Chem. Soc. Rev.* **2016**, *45*, 6597-6626; (c)

Colombeau, L.; Acherar, S.; Baros, F.; Arnoux, P.; Gazzali, A. M.; Zaghdoudi, K.; Toussaint, M.; Vanderesse, R.; Frochot, C., Inorganic Nanoparticles for Photodynamic Therapy. In *Light-Responsive Nanostructured Systems for Applications in Nanomedicine*, Sortino, S., Ed. 2016; Vol. 370, pp 113-134; (d) Bacellar, I. O. L.; Tsubone, T. M.; Pavani, C.; Baptista, M. S., Photodynamic Efficiency: From Molecular Photochemistry to Cell Death. *Int. J. Mol. Sci.* **2015**, *16*, 20523-20559.

2. (a) Schmidt, R., Quantitative determination of $^1\Sigma_g^+$ and $^1\Delta_g$ singlet oxygen in solvents very different polarity. General energy gap law for rate constants of electronic energy transfer to and from O₂ in the absence of charge-transfer interactions. *J. Phys. Chem. A* **2006**, *110*, 10369-10369; (b) Cui, G. L.; Fang, W. H., State-specific heavy-atom effect on intersystem crossing processes in 2-thiothymine: A potential photodynamic therapy photosensitizer. *J. Chem. Phys.* **2013**, *138*, 044315; (c) Cui, G. L.; Thiel, W., Intersystem Crossing Enables 4-Thiothymidine to Act as a Photosensitizer in Photodynamic Therapy: An Ab Initio QM/MM Study. *J. Phys. Chem. Lett.* **2014**, *5*, 2682-2687; (d) Martínez-Fernández, L.; Corral, I.; Granucci, G.; Persico, M., Competing ultrafast intersystem crossing and internal conversion: a time resolved picture for the deactivation of 6-thioguanine. *Chem. Sci.* **2014**, *5*, 1336-1347; (e) Chiodo, S. G.; Russo, N., DFT spin-orbit coupling between singlet and triplet excited states: A case of psoralen compounds. *Chem. Phys. Lett.* **2010**, *490*, 90-96; (f) Tatchen, J.; Marian, C. M., Vibronic absorption, fluorescence, and phosphorescence spectra of psoralen: a quantum chemical investigation. *Phys. Chem. Chem. Phys.* **2006**, *8*, 2133-2144.

3. (a) Boggio-Pasqua, M.; López Vidal, M.; Garavelli, M., Theoretical mechanistic study of self-sensitized photo-oxygenation and singlet oxygen thermal release in a dimethyldihydropyrene derivative. *J. Photochem. Photobiol. A* **2017**, *333*, 156-164; (b) Sumita, M.; Morihashi, K., Theoretical Study of Singlet Oxygen Molecule Generation via an Exciplex with Valence-Excited Thiophene. *J. Phys. Chem. A* **2015**, *119*, 876-883; (c) Martínez-Fernández, L.; González-Vázquez, J.; González, L.; Corral, I., Time-Resolved Insight into the Photosensitized Generation of Singlet Oxygen in Endoperoxides. *J. Chem. Theory Comput.* **2015**, *11*, 406-414; (d) Asturiol, D.; Barbatti, M., Electronic states of porphycene-O₂ complex and photoinduced singlet O₂ production. *J. Chem. Phys.* **2013**,

139; (e) Coitiño, E. L.; Mella, A.; Cárdenas-Jirón, G. I., Theoretical assessment of the photosensitization mechanisms of porphyrin–ruthenium(II) complexes for the formation of reactive oxygen species. *J. Photochem. Photobiol. A* **2014**, *294*, 68-74; (f) Serrano-Pérez, J. J.; Olaso-González, G.; Merchán, M.; Serrano-Andrés, L., Singlet oxygen generation in PUVA therapy studied using electronic structure calculations. *Chem. Phys.* **2009**, *360*, 85-96.

4. (a) Xie, B. B.; Liu, X. Y.; Fang, Q.; Fang, W. H.; Cui, G. L., The Position of the N Atom Plays a Significant Role for Excited-State Decay of Heterocycles. *J. Phys. Chem. Lett.* **2017**, *8*, 1019-1024; (b) Martinez-Fernandez, L.; Gonzalez, L.; Corral, I., An ab initio mechanism for efficient population of triplet states in cytotoxic sulfur substituted DNA bases: the case of 6-thioguanine. *Chem. Commun.* **2012**, *48*, 2134-2136; (c) Mai, S.; Pollum, M.; Martinez-Fernandez, L.; Dunn, N.; Marquetand, P.; Corral, I.; Crespo-Hernandez, C. E.; Gonzalez, L., The origin of efficient triplet state population in sulfur-substituted nucleobases. *Nat. Commun.* **2016**, *7*; (d) Bai, S.; Barbatti, M., Why Replacing Different Oxygens of Thymine with Sulfur Causes Distinct Absorption and Intersystem Crossing. *J. Phys. Chem. A* **2016**, *120*, 6342-6350.

5. Bai, S.; Barbatti, M., On the decay of the triplet state of thionucleobases. *Phys. Chem. Chem. Phys.* **2017**, *19*, 12674-12682.

6. Ogilby, P. R., Singlet oxygen: there is indeed something new under the sun. *Chem. Soc. Rev.* **2010**, *39*, 3181-3209.

7. (a) You, Z. Q.; Hsu, C. P., Ab Initio Study on Triplet Excitation Energy Transfer in Photosynthetic Light-Harvesting Complexes. *J. Phys. Chem. A* **2011**, *115*, 4092-4100; (b) Scholes, G. D., Long-range resonance energy transfer in molecular systems. *Annu. Rev. Phys. Chem.* **2003**, *54*, 57-87; (c) Subotnik, J. E.; Vura-Weis, J.; Sodt, A. J.; Ratner, M. A., Predicting Accurate Electronic Excitation Transfer Rates via Marcus Theory with Boys or Edmiston-Ruedenberg Localized Diabatization. *J. Phys. Chem. A* **2010**, *114*, 8665-8675.

8. (a) Yost, S. R.; Lee, J.; Wilson, M. W. B.; Wu, T.; McMahan, D. P.; Parkhurst, R. R.; Thompson, N. J.; Congreve, D. N.; Rao, A.; Johnson, K.; Sfeir, M. Y.; Bawendi, M. G.; Swager, T. M.; Friend, R. H.; Baldo, M. A.; Van Voorhis, T., A transferable model for singlet-fission kinetics. *Nature Chemistry* **2014**, *6*, 492-497; (b) Yang, C. H.; Hsu, C. P.,

First-Principle Characterization for Singlet Fission Couplings. *J. Phys. Chem. Lett.* **2015**, *6*, 1925-1929; (c) Wu, Q.; Cheng, C.-L.; Van Voorhis, T., Configuration interaction based on constrained density functional theory: A multireference method. *J. Chem. Phys.* **2007**, *127*; (d) Kolomeisky, A. B.; Feng, X. T.; Krylov, A. I., A Simple Kinetic Model for Singlet Fission: A Role of Electronic and Entropic Contributions to Macroscopic Rates. *J. Phys. Chem. C* **2014**, *118*, 5188-5195.

9. (a) Harvey, J. N.; Aschi, M., Spin-forbidden dehydrogenation of methoxy cation: a statistical view. *Phys. Chem. Chem. Phys.* **1999**, *1*, 5555-5563; (b) Harvey, J. N.; Aschi, M.; Schwarz, H.; Koch, W., The singlet and triplet states of phenyl cation. A hybrid approach for locating minimum energy crossing points between non-interacting potential energy surfaces. *Theor. Chem. Acc.* **1998**, *99*, 95-99.

10. Harvey, J. N., Understanding the kinetics of spin-forbidden chemical reactions. *Phys. Chem. Chem. Phys.* **2007**, *9*, 331-343.

11. Kuramochi, H.; Kobayashi, T.; Suzuki, T.; Ichimura, T., Excited-State Dynamics of 6-Aza-2-thiothymine and 2-Thiothymine: Highly Efficient Intersystem Crossing and Singlet Oxygen Photosensitization. *J. Phys. Chem. B* **2010**, *114*, 8782-8789.

12. Gobbo, J. P.; Borin, A. C., On The Population of Triplet Excited States of 6-Aza-2-Thiothymine. *J. Phys. Chem. A* **2013**, *117*, 5589-5596.

13. (a) Glowacki, D. R.; Liang, C. H.; Morley, C.; Pilling, M. J.; Robertson, S. H., MESMER: An Open-Source Master Equation Solver for Multi-Energy Well Reactions. *J. Phys. Chem. A* **2012**, *116*, 9545-9560; (b) Robertson, S. H.; Pilling, M. J.; Jitariu, L. C.; Hillier, I. H., Master equation methods for multiple well systems: application to the 1,2-pentyl system. *Phys. Chem. Chem. Phys.* **2007**, *9*, 4085-4097; (c) Miller, J. A.; Klippenstein, S. J., Master equation methods in gas phase chemical kinetics. *J. Phys. Chem. A* **2006**, *110*, 10528-10544; (d) Pilling, M. J.; Robertson, S. H., Master equation models for chemical reactions of importance in combustion. *Annu. Rev. Phys. Chem.* **2003**, *54*, 245-275.

14. (a) Bredas, J. L.; Beljonne, D.; Coropceanu, V.; Cornil, J., Charge-transfer and energy-transfer processes in π -conjugated oligomers and polymers: A molecular picture. *Chem. Rev.* **2004**, *104*, 4971-5003; (b) Bixon, M.; Jortner, J., Electron transfer: from

isolated molecules to biomolecules. *Adv. Chem. Phys.* **1999**, *106*, 35-202; (c) Toniolo, A.; Persico, M., Efficient calculation of Franck–Condon factors and vibronic couplings in polyatomics. *J. Comput. Chem.* **2001**, *22*, 968-975.

15. (a) Gessner, F.; Scaiano, J. C., Importance of entropy terms in triplet energy-transfer equilibria. *J. Am. Chem. Soc.* **1985**, *107*, 7206-7207; (b) Bredas, J. L.; Beljonne, D.; Coropceanu, V.; Cornil, J., Charge-transfer and energy-transfer processes in pi-conjugated oligomers and polymers: A molecular picture. *Chem. Rev.* **2004**, *104*, 4971-5003.

16. (a) Ornsø, K. B.; Jonsson, E. O.; Jacobsen, K. W.; Thygesen, K. S., Importance of the Reorganization Energy Barrier in Computational Design of Porphyrin-Based Solar Cells with Cobalt-Based Redox Mediators. *J. Phys. Chem. C* **2015**, *119*, 12792-12800; (b) Sumi, H.; Marcus, R. A., Dynamic effects in electron-transfer reactions. *J. Chem. Phys.* **1986**, *84*, 4894-4914.

17. Schweitzer, C.; Schmidt, R., Physical Mechanisms of Generation and Deactivation of Singlet Oxygen. *Chem. Rev.* **2003**, *103*, 1685-1757.

18. Li, S. L.; Truhlar, D. G.; Schmidt, M. W.; Gordon, M. S., Model space diabaticization for quantum photochemistry. *J. Chem. Phys.* **2015**, *142*, 064106.

19. Köppel, H., Conical Intersections - Theory, Computation and Experiment. In *Diabatic representation: methods for construction of diabatic electronic states*, Domcke, W.; Yarkony, D. R.; Köppel, H., Eds. World Scientific: Singapore, 2011; pp 175-204.

20. Lischka, H.; Dallos, M.; Szalay, P. G.; Yarkony, D. R.; Shepard, R., Analytic evaluation of nonadiabatic coupling terms at the MR-CI level. I. Formalism. *J. Chem. Phys.* **2004**, *120*, 7322-7329.

21. Baer, M., *Beyond Born-Oppenheimer: Electronic Nonadiabatic Coupling Terms and Conical Intersections*. John Wiley & Sons: New Jersey, 2006.

22. Barbatti, M.; Belz, S.; Leibscher, M.; Lischka, H.; Manz, J., Sensitivity of femtosecond quantum dynamics and control with respect to non-adiabatic couplings: Model simulations for the cis-trans isomerization of the dideuterated methaniminium cation. *Chem. Phys.* **2008**, *350*, 145-153.

23. (a) Marian, C. M., Spin-orbit coupling and intersystem crossing in molecules. *WIREs: Comp. Mol. Sci.* **2012**, *2*, 187-203; (b) N. Harvey, J.; Aschi, M., Spin-forbidden dehydrogenation of methoxy cation: a statistical view. *Phys. Chem. Chem. Phys.* **1999**, *1*, 5555-5563; (c) Glowacki, D. R.; Liang, C.-H.; Morley, C.; Pilling, M. J.; Robertson, S. H., MESMER: An Open-Source Master Equation Solver for Multi-Energy Well Reactions. *J. Phys. Chem. A* **2012**, *116*, 9545-9560.
24. Finley, J.; Malmqvist, P. A.; Roos, B. O.; Serrano-Andrés, L., The multi-state CASPT2 method. *Chem. Phys. Lett.* **1998**, 288, 299-306.
25. Ghigo, G.; Roos, B. O.; Malmqvist, P.-A., A modified definition of the zeroth-order Hamiltonian in multiconfigurational perturbation theory (CASPT2). *Chem. Phys. Lett.* **2004**, *396*, 142-149.
26. Lischka, H.; Muller, T.; Szalay, P. G.; Shavitt, I.; Pitzer, R. M.; Shepard, R., COLUMBUS-A Program System for Advanced Multireference Theory Calculations. *Wiley Interdiscip. Rev.-Comput. Mol. Sci.* **2011**, *1*, 191-199.
27. (a) D G Truhlar, a.; Garrett, B. C., Variational Transition State Theory. *Annu. Rev. Phys. Chem.* **1984**, *35*, 159-189; (b) Garrett, B. C.; Truhlar, D. G., Chapter 5 - Variational transition state theory A2 - Dykstra, Clifford E. In *Theory and Applications of Computational Chemistry*, Frenking, G.; Kim, K. S.; Scuseria, G. E., Eds. Elsevier: Amsterdam, 2005; pp 67-87.
28. Baier, J.; Fuß, T.; Pöllmann, C.; Wiesmann, C.; Pindl, K.; Engl, R.; Baumer, D.; Maier, M.; Landthaler, M.; Bäuml, W., Theoretical and experimental analysis of the luminescence signal of singlet oxygen for different photosensitizers. *Journal of Photochemistry and Photobiology B: Biology* **2007**, *87*, 163-173.

TOC graph

